JMEPEG (2012) 21:907–914
DOI: 10.1007/s11665-011-9987-z

1059-9495/$19.00

A Comparative Study on Nd:YAG Laser Cutting of Steel and Stainless Steel Using Continuous, Square, and Sine Waveforms

K.H. Lo

(Submitted September 8, 2010; in revised form March 24, 2011)

Laser cutting with the sine waveform is seldom reported. This article is a comparative study on Nd:YAG laser cutting using the continuous (CW), square, and sine waveforms. The materials used in this study were steel and stainless steel. It has been found that the cutting capability, in descending order, is: CW > sine > square. The cutting of steel (C ~0.3 wt.%) and AISI304 austenitic stainless steel may be satisfactorily described by the Steen model, irrespective of waveform. Steel is slightly easier to cut than stainless steel. Limitations of the present study are discussed and suggestions for future work are made.

Keywords cutting, Nd:YAG, stainless steel, steel

1. Introduction

Since its debut in the 1960s, laser cutting has made great strides. A wide variety of materials has been shown to be laser cuttable. These include aluminum alloy, Ni-base superalloy (Ref 1, 2), steel (Ref 3), and ceramics (Ref 4-9). Very thick plates (40 mm) can be cut with good cut-surface quality (Ref 10).

Arguably speaking, the most widely used lasers in the industry are CO_2 and Nd:YAG lasers (Ref 11, 12). Nd:YAG laser offers many advantages over its CO_2 counterpart. Some of these are: a 10-fold shorter wavelength (1.064 μm), compactness in size, and amenability to delivery through optical fibers (Ref 11). Being able to operate in the pulsed mode is another strength of Nd:YAG laser. A number of recent publications on Nd:YAG laser cutting using the continuous waveform (CW) (Ref 13-15) and the pulsed waveform, i.e., the square waveform (Ref 13, 16, 17) are available in the literature. It is no exaggeration that the effects of process parameters (such as gas pressure and type, laser power, pulse repetition rate) have been thoroughly assessed.

For Nd:YAG laser, besides the CW and pulsed (square) waveforms, new designs are also capable of generating the sine waveform. One such laser is the JK MultiWave™ Laser (Model MW500) from Lumonics. As far as the author is aware, there has been virtually no report on cutting with the sine waveform. In addition, it seems that no comparative study has been conducted on the CW, the square, and the sine waveforms. The present work is such a comparative study.

K.H. Lo, Department of Electromechanical Engineering, Faculty of Science and Technology, The University of Macau, Macau, China. Contact e-mail: khlo@umac.mo.

As carbon steels and stainless steels are used extensively and because a lot of literature on laser cutting (using the continuous and pulsed lasers) is devoted to these two materials. The present work will also focus on the laser cuttability of these two materials.

2. Experimental Details

The materials used in this work were a low-carbon steel (C ~0.3 wt.%) and the AISI304 austenitic stainless steel. The laser used was a Lumonics© JK MultiWave™ MW500 Nd:YAG laser that was pumped by two quartz tubes (flashlamps). In the CW mode, the maximum power reachable by the laser was 500 W.

A HeNe laser beam, which was transmitted in the same optical path of the invisible Nd:YAG laser beam, was used for focusing purposes. The helium laser beam was focused (and so was the Nd:YAG laser beam) on the plate surfaces, having a spot size of about 0.75 mm in diameter (as measured by using a caliper). The cutting head was tilted about 10° off the normal of the plate surfaces to avoid fiber damage by laser backscattering. Chen has shown that oxygen-reactive laser cutting is very sensitive to gas purity (Ref 18). In order to minimize this effect, the assist gas used was high-purity oxygen (99.99%). The oxygen was fed to the laser-material interaction zone by a coaxial, conical nozzle. The stand-off distance between the nozzle tip and the plate surfaces was about 1 mm. The pressure of the assist gas was kept at 8 bar. Because of the setup of the laser system, the flow rate could not be varied too much.

Nominal laser power values are used in this work, instead of the real laser power values at the sample surfaces (because of a lack of the requisite equipment). The actual laser power delivered to the plate surfaces would be smaller, inasmuch as there were bound to be losses as the laser beam traveled through the optics. Nevertheless, because the same laser source and the same optics were used, the three types of waveforms would be affected more or less to the same extent. Therefore, using nominal laser power values does not affect the comparative

discussions in subsequent sections, insofar as all the lines in the figures would have been shifted proportionately had real power been used. At the time when this work was done, the laser machine had just been newly installed and so it had been well calibrated by the manufacturer. The mode of the laser beam was not checked. However, burn tests using photosensitive films showed that the laser beam was the most intense at the center, with its intensity dropping off gradually radially. During the cutting trials, photosensitive films were used regularly to check the intensity distribution of the laser beam.

For both of the square and sine waveforms, the same average power level ($P_{\text{Average}} = 400$ W), peak power ($P_{\text{Peak}} = 800$ W), and frequency ($f = 350$ Hz) were used. Although, the maximum average power reachable by the laser in the CW mode was 500 W, just 400 W was used in order to avoid stressing the laser system and optics, and to guard against mode corruption (Ref 19). A peak power of 800 W was chosen because this peak value was the highest obtainable with the sine waveform when the average power was fixed at 400 W. When the square waveform is used, however, the maximum peak power could reach 1250 W. Nevertheless, for comparison purposes, a peak power of 800 W was chosen for the square waveform, too. The pulse width (d) of the square waveform was about 1.43 ms $\left(P_{\text{Peak}} = P_{\text{Average}}/d \cdot f\right)$. To obtain cuts of good quality, there must be sufficient overlap between adjacent laser pulses, yet the overlap must not be excessive, if severe sideburns and melting are to be staved off (Ref 20). It was found that a frequency of 350 Hz was sufficient to ensure an adequate overlap between adjacent pulses for the square waveform even for the highest cutting speed used. When the cutting speed was low, the pulses must overlap each other a lot at 350 Hz. However, the plates did not seem to suffer excessive sideburns and melting. Consequently, this frequency was chosen.

The evaluation of laser cut quality is still very subjective, especially for thick plates (Ref 21). Some criteria have been proposed by different authors and these include roughness of cut surface (Ref 22), minimum edge rounding (Ref 21), kerf width (Ref 15), kerf taper and deviation (Ref 1, 2), metallurgical change at cut surface (Ref 22), and degree of sideburns (Ref 10). Nevertheless, it is difficult, if not impossible, to produce cuts that can meet all of the criteria. Optimization of some of the good cut criteria (kerf consistence and taper) is usually attained at the expense of others (e.g., kerf width) (Ref 2). This tradeoff problem is inherent to multi-objective optimization. Consequently, only some of the above-mentioned criteria were adopted to judge what constituted good cuts in the present work.

Thick plates cut by laser is regarded as being of good quality if they are free from top and bottom dross (dross is the once molten material that re-solidified and adhered to the plates), have fine and uniform striations, are gouge-free, and have minimum edge rounding (Ref 21). Although the plates used in the present work were not thick (1-4 mm), the thick-plate criteria are certainly applicable. Consequently, these criteria were adopted to judge what constituted good cuts in the present work. Besides, cuts having excessive sideburns were considered bad, no matter whether the afore-mentioned criteria were met or not. For a certain combination of power level and plate thickness, there is usually a range of useable cutting speeds. In this work, the maximum cutting speed is used.

No metallurgical work was done to gauge the extent of the heat-affected zones (HAZs) of the samples. The widest color changes induced in the stainless steel samples were found to extend to about 0.8 mm away from the cut edge for samples cut with a low speed and a high power. Some microhardness measurements were done on the stainless steel samples and it was found that the hardness values seemed to be unaffected just off the color change zones. Roughly, it may be estimated that the widest HAZ in the samples was about 0.8 mm in width. A Hitachi S-3400N, Type I scanning electron microscope was used to examine the cut edges of the samples.

The surface oxide scale of both steel plates and stainless steel plates were not ground away before laser cutting. The plates were put into a desiccator about 2 weeks before the cutting trials, with an eye to eliminating any entrapped moisture in the oxide scales. Therefore, the possibility of vapor interfering with the laser-material interaction was minimized.

3. Results and Discussion

3.1 The Cut Surfaces

Figure 1 shows bad cuts containing severe dross and gouges in the plate bottoms. Good cuts were easily obtained from plates thinner than 2 mm. Since the maximum average power used was just 350 W, the 3 and 4 mm plates were trickier to cut. For the 4 mm plate, the surface quality as shown in Fig. 2 was considered acceptable, and this cut quality is in fact comparable to those conventionally achievable in thicker plates. It has been pointed out that the use of oxygen would lead to wide kerfs and rough surfaces (Ref 13). Since the oxygen used in the present work was of high purity, the striations shown in Fig. 2 are not overly unacceptable. Relatively straight striations extended from the top through to the bottom, and the bottom was nearly dross free. In addition, the cut edges were straight.

No cracks could be found with the naked eye in all of the samples. However, small cracks could be seen when the cut edges were examined under the scanning electron microscope.

Figure 3 shows the cut edge of a steel sample that was considered bad. It may be seen that the cut edge is quite rough. Small globules of once molten material could be seen to adhere to the cut edge. When viewed at a higher magnification,

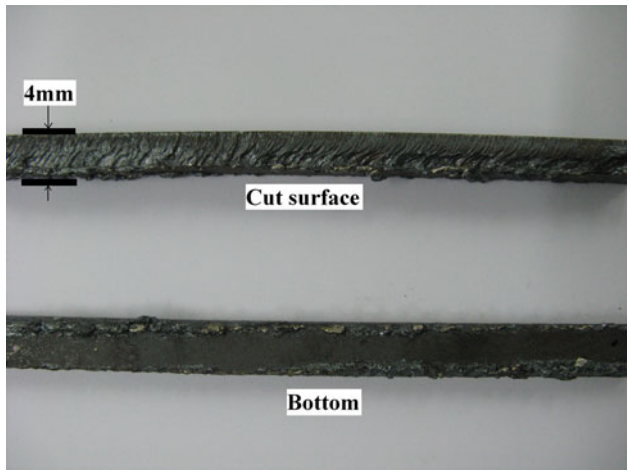

Fig. 1 Side view and bottom view of bad cuts of steel plates

Fig. 2 Cut surface considered good in the 4 mm steel plates

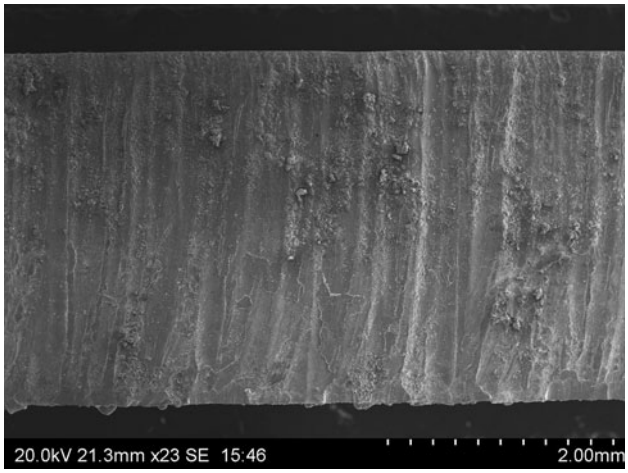

Fig. 5 The cut edge of a carbon-steel sample that was considered good

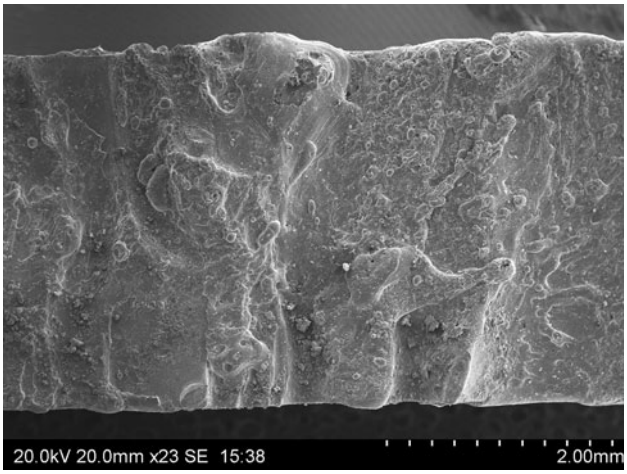

Fig. 3 The cut edge of a carbon-steel sample that was considered bad

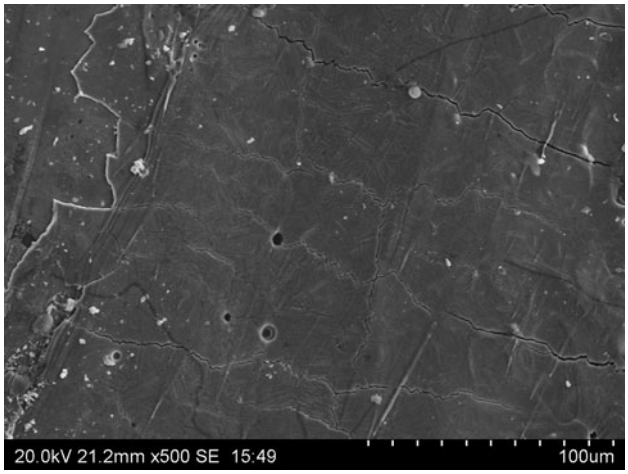

Fig. 6 Small cracks on the cut edge of a good carbon-steel steel sample

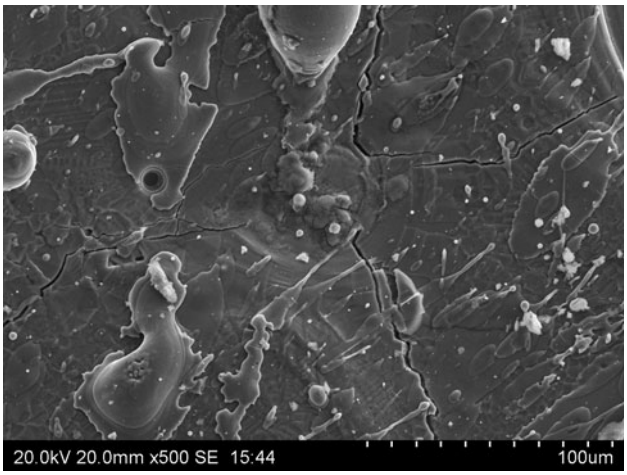

Fig. 4 Small cracks and globules on the cut edge of a bad carbon-steel steel sample

the globules can be seen more clearly and small cracks are revealed (Fig. 4). These small cracks are believed to be associated mostly with the cracking of the surface oxide on the cut edge.

For carbon-steel samples that are considered good in the present work, the cut edge is much smoother (Fig. 5). The reduction in surface roughness is obvious when Fig. 4 and 6 are compared. Small globules of once molten material may still be found to clink to the cut edge. However, overall, their number was lower than that in the bad samples. Again, small cracks could be found on the cut edge and these are, as mentioned, believed to be associated with the cracking of the surface oxide on the cut edge. The situation for the stainless steel samples was similar to that of the carbon-steel samples.

3.2 Cutting of Steel Plates

For steel plates, Fig. 7-9 shows that a linear relationship exists between power-thickness ratio (P/t) and maximum cutting speed (V) for all of the three types of waveforms.

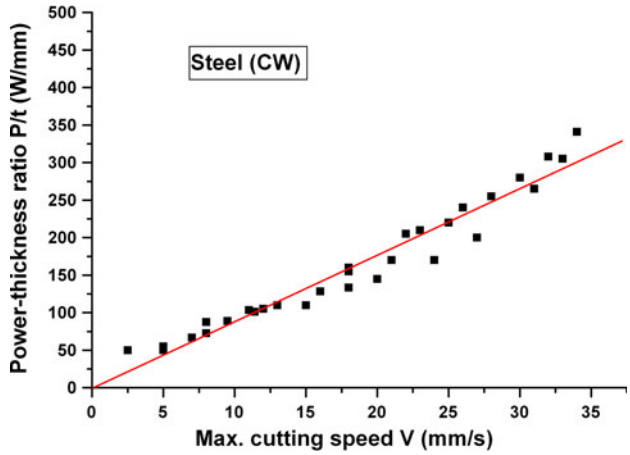

Fig. 7 The (P/t)-V line of steel cut using the continuous waveform

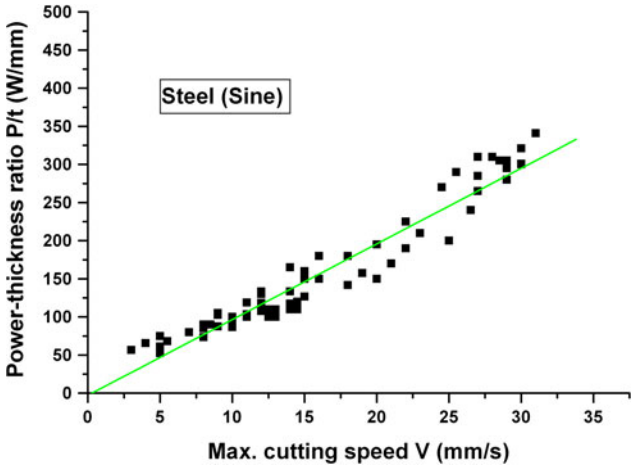

Fig. 8 The (P/t)-V line of steel cut using the sine waveform

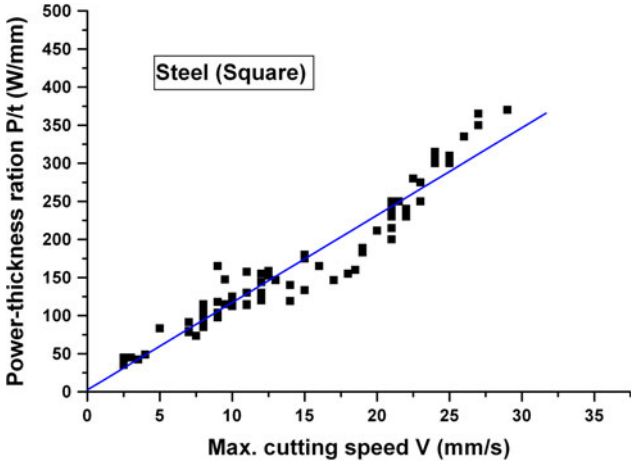

Fig. 9 The (P/t)-V line of steel cut using the square waveform

The linearity between (P/t) and V is best explained by adopting the simple, yet reasonable, model proposed by Steen (Ref 11).

Table 1 Average severance energies of steel and stainless steel for the three waveforms (J/mm^2)

	CW	Sine	Square
Steel	8.871	9.928	11.467
Stainless steel	9.280	11.964	12.852

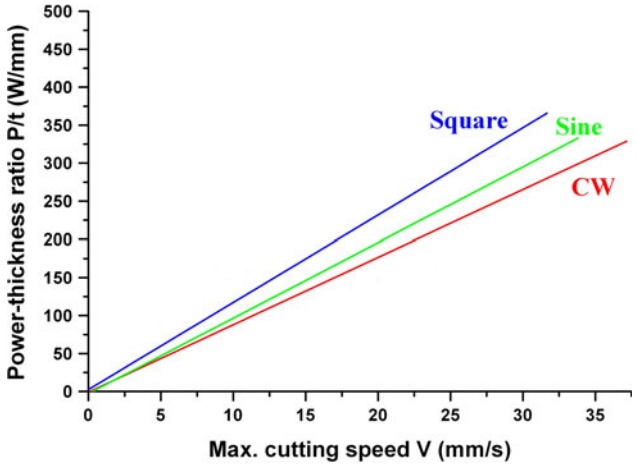

Fig. 10 Comparison of the (P/t)-V lines of steel cut using the CW, sine, and square waveforms (For clarity, data points as indicated in Fig. 7-9 are omitted)

$$\frac{P}{t} = \left\{\frac{w \cdot \rho}{\eta}[C_P(T_M - T_O) + L_F + m'L_V]\right\} \cdot V$$
$$= f(\text{material}) \cdot V = \text{Constant} \cdot V, \qquad \text{(Eq 1)}$$

where w is the kerf width, ρ is the density of material, η is the laser-material coupling coefficient, C_P is the heat capacity of material, T_M is the melting temperature of material, T_O is the ambient temperature, L_F is the latent heat of fusion of material, m' is the fraction of material that is vaporized, L_V is the latent heat of vaporization of material, and f(material) is the severance energy, which is a constant for a given material.

Here, the severance energy (the energy required to severe the material as the laser beam passes the material) is the sum of the energies needed to (1) bring the material to the melting point, (2) fuse the material, and (3) vaporize the molten material. The Steen model was developed for fusion cutting, i.e., without taking into account the contribution from the exothermic oxidation reaction involving molten iron and oxygen. This model has been shown to be accurate for slate (Ref 23), which is only very weakly oxidisable. Nevertheless, Steen (Ref 11) and Black (Ref 24) have demonstrated that the model can fit well to the oxygen-reactive cutting data obtained by other researchers. The present data confirm the validity of the Steen model for reactive laser cutting, too.

The severance energy of steel (with oxygen as the assist gas) falls within 4 and 13 J/mm^2 with an average of 5.7 J/mm^2. The severance energies of steel, as indicated by their slopes in Fig. 7-9, all fall within these ranges (Table 1).

The severance energies indicate that the capability of cutting steel of the three waveforms, in descending order, is: CW > sine > square. This is indeed the case if Fig. 7-9 are lumped into a single figure (Fig. 10).

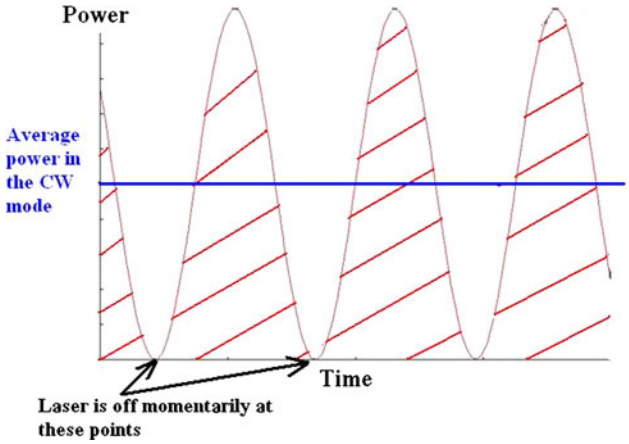

Fig. 11 Schematic depicting the sine waveform

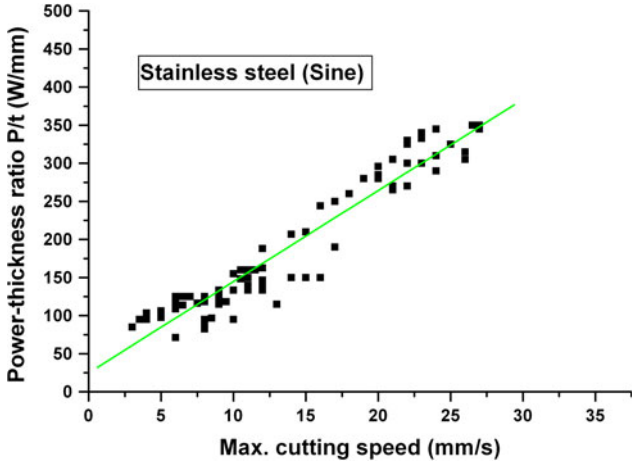

Fig. 13 The (P/t)-V line of AISI304 cut using the sine waveform

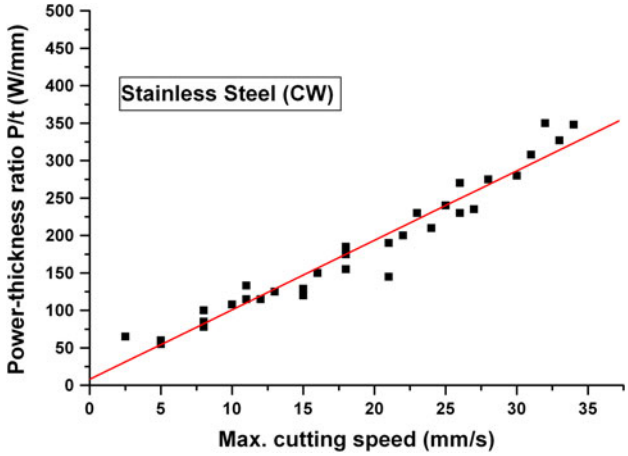

Fig. 12 The (P/t)-V line of AISI304 cut using the continuous waveform

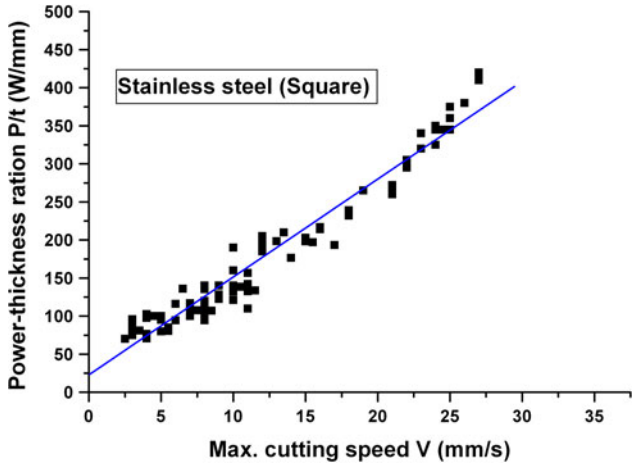

Fig. 14 The (P/t)-V line of AISI304 cut using the square waveform

Because of the exothermic oxidation reaction, steel is very amenable to O_2-reactive laser cutting. When the CW waveform is used, the continuous supply of extra energy from the exothermic oxidation reaction aids enormously the cutting process. For the square waveform, laser irradiation undergoes on and off periods. It has been shown that during the laser off periods, the exothermic reaction may not proceed non-stop and so is not efficient (Ref 20). The sine waveform, as demonstrated in Fig. 11, is sort of an intermediate between the CW and the square waveforms. The supply of laser energy is only off momentarily (as opposed to the square waveform that is off for discrete, short durations). Although the laser energy may drop to very low levels, the laser supply never stops (except momentarily at points as indicated in Fig. 11). Hence, with the sine waveform, the exothermic may proceed more efficiently than with the square waveform.

3.3 Cutting of Austenitic Stainless Steel Plates

Results on the cutting of AISI304 austenitic stainless steel plates are similar to those on steel plates, i.e., the relationship between (P/t) and V is linear (Fig. 12-14), and that the order of cutting capability is still CW > sine > square (Fig. 15).

For stainless steel, the range of severance energy is 7 and 22 J/mm^2 with an average of 10 J/mm^2 (Ref 11). Table 1 shows that the severance energies of AISI304 obtained in the present work fall within this range.

3.4 Comparison of Cutting of Steel and Stainless Steel Using the Three Waveforms

Table 1 shows that steel is easier to cut than stainless steel for all of the three waveforms, on grounds of the former's lower severance energies. Superposing the (P/t)-V lines of steel and stainless steel obviates this trend (Fig. 16-18).

In the CW mode, Fig. 16 shows that the steel and the stainless steel may be cut at relatively the same rate. This result conforms to that obtained by Carroll and Rothenflue (Ref 25). These authors found that steel and stainless steel might be cut at roughly the same scan speed with a chemical oxygen-iodine laser (COIL), whose wavelength (1.315 μm) is close to the Nd:YAG wavelength (1.064 μm). Irrespective of waveform,

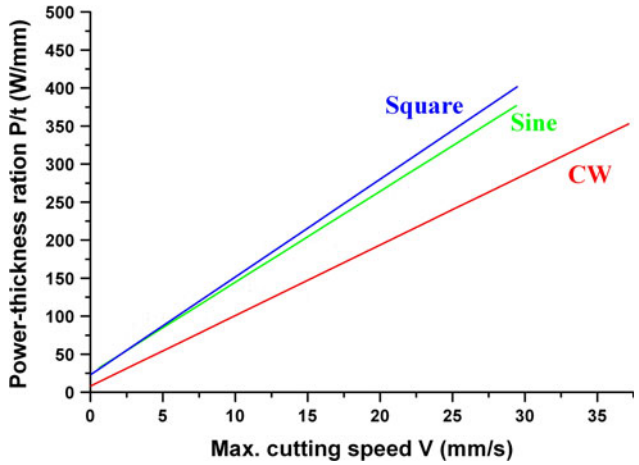

Fig. 15 Comparison of the (P/t)-V lines of AISI304 cut using the CW, sine, and square waveforms (For clarity, data points as indicated in Fig. 12-14 are omitted)

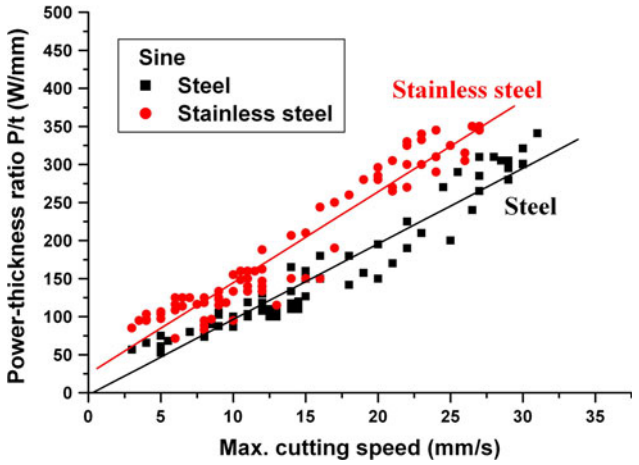

Fig. 17 Comparison of the sine waveform in cutting steel and stainless steel

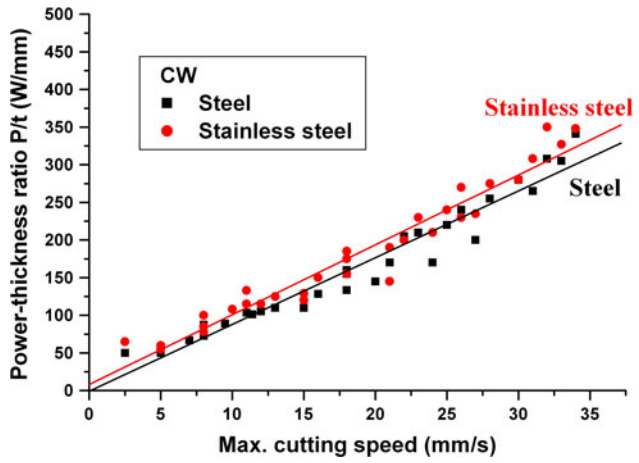

Fig. 16 Comparison of the CW waveform in cutting steel and stainless steel

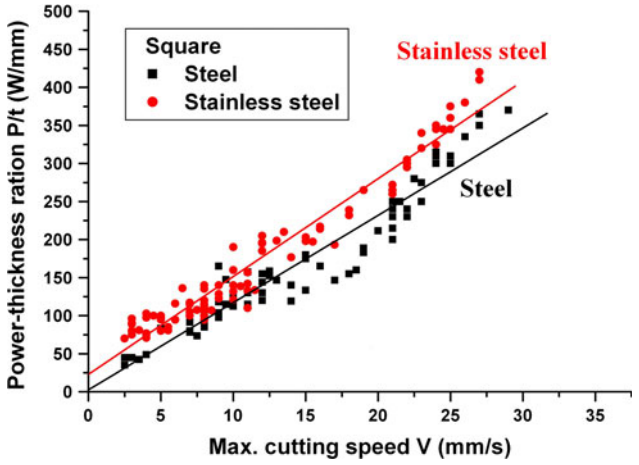

Fig. 18 Comparison of the square waveform in cutting steel and stainless steel

steel exhibits a better reactive laser cuttability than does stainless steel.

The better laser cuttability of steel may be explained as follows: first, although Steen suggests that the exothermic oxidation reaction may contribute up to 60% of the cutting energy for *both* steel and stainless steel (Ref 11), it is generally accepted that the exothermic reaction is less efficient in stainless steel compared with unalloyed steel (Ref 19, 26). This is because the oxidation reaction is frustrated by the formation of the impermeable oxide Cr_2O_3, which seals the underlying material and so will hinder it from reacting with the incoming oxygen gas jet (Ref 19). Second, the absorptivity of laser is higher in steel than in stainless steel. It is to be noted that although the thermal conductivity of stainless steel is higher than that of steel, this cannot offset the lower absorptivity and less intense oxidation reaction of the former. Hence, the overall cuttability of stainless steel is inferior to that of steel (Fig. 16-18).

As molten material in the cut zone is blown out by the assist gas, it is not unreasonable to ignore the latent-heat-of-vaporization term in the Steen model (Ref 11, 24). The simplified Steen model is then as follows. A higher Φ implies a harder-to-cut material (Ref 24):

$$\frac{P}{t \cdot V} = \frac{w \cdot \rho}{\eta}[C_P(T_M - T_O) + L_F] = \Phi \qquad \text{(Eq 2)}$$

The kerf widths (w) of steel plates and stainless steel plates did not differ too much in the present work and so $w_{Stainless\_steel} \approx w_{Steel}$ may be assumed. Carroll and Rothenflue estimated that the absorptivity of iron should be about 3% higher than the absorptivity of stainless steel at the Nd:YAG wavelength (Ref 25). They also estimated that the absorptivity of iron is roughly the same as that of steel. Therefore, it may be assumed that $\eta_{Stainless\_steel} = 0.97 \cdot \eta_{Steel}$. When the thermophysical properties in Table 2 are substituted into the simplified Steen model (Eq 2), it may be found that $\Phi_{Stainless\_steel}/\Phi_{Steel} \approx 1.12$, which means stainless steel is slightly harder to cut than steel.

It must be pointed out that the physical properties will change with temperature. Therefore, more accurate comparisons may be made on the cutting capabilities of the three

Table 2 Thermophysical properties of stainless steel and steel

	Density, ρ (kg m^{-3})	Specific heat, C_P (J kg^{-1} K^{-1})	Melting temperature, T_M (K)	Latent heat of fusion, L_F (J kg^{-1})
AISI304 (Ref 7)	8030	500	1723	300
Steel[#]	7800	460	1808	272

[#]Values obtained from Engineers Edge (http://www.engineersedge.com/properties_of_metals.htm) and The Engineering Toolbox (http://www.engineeringtoolbox.com/fusion-heat-metals-d_1266.html)

waveforms if relations describing the temperature-dependence of the thermophysical properties are used in Eq 2.

4. Comments on the Limitations of the Present Study and Suggestions for Future Work

The present work is a preliminary attempt aiming at elucidating the cutting capability of the sine waveform. The criteria chosen for judging what constituted good cuts were (1) through-the-thickness cuts with no (minimum) dross and (2) relatively uniform striations with square cut edges. As mentioned in Section 2, other criteria could have been used and these might be the degree of sideburns, roughness of cut surfaces, kerf width, and the like. Although cuts sustaining excess sideburns were at times rejected as bad cuts, it was found that cuts in stainless steel plates satisfying the chosen criteria might suffer from noticeable sideburns (e.g., a kerf width of 1 mm with a HAZ of about 0.8 mm in width on either side of the cut). However, since the extent of sideburns was not used as a main yardstick in the present work, some cuts with noticeable sideburns were still judged good. Therefore, it is possible that when more stringent criteria are used (such as the inclusion of the degree of sideburns), the present results might need modification.

Nevertheless, it has to be emphasized that this kind of problem is inherent to laser cutting, which is a multiobjective optimization problem. It is impossible to satisfy all of the objectives at the same time. That is, the optimization of some criteria will lead to a deterioration in the other criteria. It is thus informative to select other criteria (e.g., narrow kerf width) and repeat the cutting tests, with the view of comparing the cutting capabilities of the three waveforms under the new set of good cut criteria.

To the best knowledge of the author, the effects of the sine waveform on kerf width, microstructures in the HAZ, and striation patterns have not been reported in the literature. Also, it is interesting to vary the parameters (amplitude, average power, and frequency) of the sine waveform and see how they affect its cutting capability. Finally, the application of the sine waveform to the cutting of other types of materials (reflective ones like aluminum and copper) may constitute interesting studies.

5. Conclusions

The cutting capabilities of the CW, the square waveform (i.e., the pulsed waveform), and the sine waveform of the Nd:YAG laser have been found to be, in descending order, as follows: CW > sine > square.

The CW waveform cuts the best because laser energy is incessantly supplied to the laser-material interaction zone. As a consequence, the exothermic oxidation reaction may be maintained continuously. The square waveform fares the worst because the laser is turned off periodically, thereby stunning the exothermic oxidation reaction periodically also. The sine waveform is intermediate between the CW and square waveforms, insofar as laser energy supply is almost non-stop (except momentarily as indicated in Fig. 11). Hence, the exothermic oxidation reaction may proceed more efficiently than for the square waveform.

For all of the three waveforms, steel is slightly easier to cut than stainless steel.

The cutting of steel and AISI304 austenitic stainless steel may be satisfactorily described by the Steen model.

References

1. A.K. Dubey and V. Yadava, Optimization of Kerf Quality During Pulsed Laser Cutting of Aluminium Alloy Sheet, *J. Mater. Process. Technol.*, 2008, **204**(1–3), p 412–418
2. A.K. Dubey and V. Yadava, Multi-Objective Optimization of Nd:YAG Laser Cutting of Nickel-Based Superalloy Sheet Using Orthogonal Array With Principal Component Analysis, *Opt. Laser. Eng.*, 2008, **46**(2), p 124–132
3. N. Rajaram, J.S. Ahmad, and S.H. Cheraghi, CO_2 Laser Cut Quality of 4130 Steel, *Int. J. Mach. Tools Manuf.*, 2003, **43**(4), p 351–358
4. A.N. Samant and N.B. Dahotre, Differences in Physical Phenomena Governing Laser Machining of Structural Ceramics, *Ceram. Int.*, 2009, **35**(5), p 2093–2097
5. A.N. Samant and N.B. Dahotre, Laser Machining of Structural Ceramics—A Review, *J. Eur. Ceram. Soc.*, 2009, **29**(6), p 969–993
6. A.N. Samant and N.B. Dahotre, Physical Effects of Multipass Two Dimensional Laser Machining of Structural Ceramics, *Adv. Eng. Mater.*, 2009, **11**(7), p 579–585
7. A.N. Samant and N.B. Dahotre, Three-Dimensional Laser Machining of Structural Ceramics, *J. Manuf. Process.*, 2010, **12**(1), p 1–7
8. A.N. Samant, B. Du, and N.B. Dahotre, In situ Surface Absorptivity Prediction During 1.06 μm Wavelength Low Aspect Ratio Machining of Structural Ceramics, *Phys. Status Solidi. A*, 2009, **206**(7), p 1433–1439
9. A.N. Samant and N.B. Dahotre, Absorptivity Transition in 1.06 μm Wavelength Laser Machining of Structural Ceramics, *Int. J. Appl. Ceram. Technol.*, 2011, **8**(1), p 127–139
10. W.O. Neill and J.T. Gabzdyl, New Developments in Laser-Assisted Oxygen Cutting, *Opt. Laser Eng.*, 2000, **34**(4–6), p 355–367
11. W.M. Steen, *Laser Materials Processing*, Springer, London, 1991
12. N. Tabata, S. Yagi, and M. Hishii, Present and Future of Lasers for Fine Cutting of Metal Plate, *J. Mater. Process. Technol.*, 1996, **62**(4), p 309–314
13. K. Ghany and M. Newishy, Cutting of 1.2 mm Thick Austenitic Stainless Steel Sheet Using Pulsed and CW Nd:YAG Laser, *J. Mater. Process. Technol.*, 2005, **168**(3), p 438–447

14. H.G. Salem, M.S. Mansour, Y. Badr, and W.A. Abbas, CW Nd:YAG Laser Cutting of Ultra Low Carbon Steel Thin Sheets Using O_2 Assist Gas, *J. Mater. Process. Technol.*, 2008, **196**(1–3), p 64–72
15. M. Bahar and H. Golnabi, Optimum Experimental Condition in Oxygen Gas-Assisted Low Power Nd:YAG Laser Cutting, *Mod. Phys. Lett. B*, 2009, **23**(6), p 877–890
16. M. Baumeister, K. Dickmann, and T. Hoult, Fiber Laser Micro-Cutting of Stainless Steel Sheets, *Appl. Phys. A*, 2006, **85**(2), p 121–124
17. L. Shanjin and W. Yang, An Investigation of Pulsed Laser Cutting of Titanium Alloy Sheet, *Opt. Laser Eng.*, 2006, **44**(10), p 1067–1077
18. S. Chen, The Effects of Gas Composition on the CO_2 Laser Cutting of Mild Steel, *J. Mater. Process. Technol.*, 2008, **73**(1–3), p 147–159
19. J. Powell, *CO_2 Laser Cutting*, 2nd ed., Springer, London, 1998
20. G. Thawari, J.K.S. Sundar, G. Sundararajan, and S.V. Joshi, Influence of Process Parameters During Pulsed Nd:YAG Laser Cutting of Nickel-Base Superalloys, *J. Mater. Process. Technol*, 2005, **170**(1–2), p 229–239
21. M. Manohar, CO_2 Laser Beam Cutting of Steels: Materials Issues, *J. Laser Appl.*, 2006, **18**(2), p 101–112
22. B.S. Yibas, Study of Parameters for CO_2 Laser Cutting Process, *Mater. Manuf. Process.*, 1998, **13**(1–3), p 5178–5186
23. M. Boutinguiza, J. Pou, F. Lusquinos, F. Quintero, R. Soto, M.P. Amor, K. Watkins, and W.M. Steen, CO_2 Laser Cutting of Slate, *Opt. Laser Eng.*, 2002, **37**(1), p 15–25
24. I. Black, A Comparison of Severance Energies for Reactive CO_2 Laser Cutting of Mild Steel, *Int. J. Adv. Manuf. Technol.*, 1999, **15**(11), p 832–834
25. D.L. Carroll and J.A. Rothenflue, Experimental Study of Cutting Thick Aluminium and Steel With a Chemical Oxygen-Iodine Laser Using an N_2 or O_2 Gas Assist, *Proceedings of the XI International Symposium on Gas Flow and Chemical Lasers and High Power Laser Conference*, H.J. Baker, Ed., 1997, p 758–763
26. T. Kek and J. Grum, Monitoring Laser Cut Quality Using Acoustic Emission, *Int. J. Mach. Tools Manuf.*, 2009, **49**(1), p 8–12